Wave-Coherent Air–Sea Heat Flux

FABRICE VERON

College of Marine and Earth Studies, University of Delaware, Newark, Delaware

W. KENDALL MELVILLE AND LUC LENAIN

Scripps Institution of Oceanography, University of California, San Diego, La Jolla, California

(Manuscript received 21 August 2006, in final form 9 August 2007)

ABSTRACT

Air–sea fluxes of heat and momentum play a crucial role in weather, climate, and the coupled general circulation of the oceans and atmosphere. Much progress has been made to quantify momentum transfer from the atmosphere to the ocean for a wide range of wind and wave conditions. Yet, despite the fact that global heat budgets are now at the forefront of current research in atmospheric, oceanographic, and climate problems and despite the good research progress in recent years, much remains to be done to better understand and quantify air–sea heat transfer. It is well known that ocean-surface waves may support momentum transfer from the atmosphere to the ocean, but the role of the waves in heat transfer has been ambiguous and poorly understood. Here, evidence is presented that there are surface wave–coherent components of both the sensible and the latent heat fluxes. Presented here are data from three field experiments that show modulations of temperature and humidity at the surface and at 10–14 m above the surface, which are coherent with the surface wave field. The authors show that the phase relationship between temperature and surface displacement is a function of wind speed. At a 10–12-m elevation, a wave-coherent heat transfer of $O(1)$ W m^{-2} is found, dominated by the latent heat transfer, as well as wave-coherent fractional contributions to the total heat flux (the sum of latent and sensible heat fluxes) of up to 7%. For the wind speeds and wave conditions of these experiments, which encompass the range of global averages, this wave contribution to total heat flux is comparable in magnitude to the atmospheric heat fluxes commonly attributed to the effects of greenhouse gases or aerosols. By analogy with momentum transfer, the authors expect the wave-coherent heat transfer to decay with height over scales on the order of k^{-1}, where k is the characteristic surface wavenumber; therefore, it is also expected that measurements at elevations of $O(10)$ m may underestimate the contribution of the wave-induced heat flux to the atmosphere.

1. Introduction

The coupled air–sea boundary layers play an important role in the fluxes of momentum, heat, and mass between the atmosphere and the ocean. These exchanges are crucial for the evolution of weather and climate, providing important boundary conditions for both the atmosphere and the oceans. The complex dynamics of this coupled system govern the multiple air–sea fluxes, and as a consequence, the region directly influenced by surface waves in both boundary layers, the "surface wave layer," has received considerable attention in recent years.

Early models of momentum boundary layers on both sides of the air–sea interface were strongly tied to the wealth of knowledge from laboratory and field measurements of the flow over rigid surfaces. Models of neutrally stratified flows are based on the well-known "law of the wall," which depends on the assumption of a constant stress layer and the flow depending on the distance from the wall normalized by a roughness length z_0. The roughness length parameterizes the influence of the roughness elements at the surface on the kinematics and dynamics of the flow. However, recent evidence (P. Sullivan 2004, personal communication) suggests that in low-wind conditions the momentum flux from the ocean to the atmosphere through forcing by the swell may lead to "supersmooth" surfaces in which the usual physical roughness interpretation of z_0 for the atmosphere is lost as z_0 becomes very small—

Corresponding author address: Fabrice Veron, College of Marine and Earth Studies, University of Delaware, 112C Robinson Hall, Newark, DE 19716.
E-mail: fveron@udel.edu

DOI: 10.1175/2007JPO3682.1

smaller than the smooth flow limit. In the last two decades, oceanographic research has shown that wave breaking introduces new balances that are important near the surface and may dominate those leading to the law of the wall (Sullivan et al. 2004, 2007).

Extending the constant momentum flux assumption to heat and moisture, it is possible, in the marine atmospheric boundary layer (MABL) near the lower boundary, to express the fluxes of momentum, sensible heat, and moisture as

$$\tau = \rho_a u_*^2 = \rho_a(\overline{u'w'} + \nu\overline{u}_z), \quad (1)$$

$$\mathrm{Qs} = \rho_a C_{pa}\theta_* u_* = \rho_a C_{pa}(\overline{\theta'w'} + \kappa_a\overline{\theta}_z), \quad \text{and} \quad (2)$$

$$\mathrm{Ql} = \rho_a L_v q_* u_* = \rho_a L_v(\overline{q'w'} + D\overline{q}_z), \quad (3)$$

respectively. The horizontal alongwind and vertical velocities are u and w, respectively. Here, θ is the potential temperature and q is the specific humidity. The subscripts z denote vertical differentiation, the primes indicate turbulent quantities (taken as deviations from the mean), and the overbars represent ensemble averages. The friction velocity in the air is denoted by u_*, and θ_* and q_* are the equivalent flux scales for potential temperature and specific humidity, respectively. Finally, ρ_a is the density of air, C_{pa} is the heat capacity of air, L_v is the latent heat of vaporization for air, $\nu = \mu/\rho_a$ is the air kinematic viscosity, κ_a is the diffusivity of heat, and D is the diffusivity for water vapor in air. If the flow is stratified, the classical models introduce the Monin–Obukhov length L, a new length scale, which is simply the distance from the wall at which shear production and buoyant production of turbulence are equal.

While the fluxes are constant within the lower atmospheric boundary layer, the relative importance of each term varies. For example, the viscous stress $\mu\overline{u}_z$ is important only very close to the surface in the viscous sublayer (less than 1 mm from the surface for wind speeds larger than 4 m s^{-1}), whereas within the viscous layer, the turbulent flux is nearly zero, at least over a rigid boundary. Over a moving wavy boundary, however, the deviations from the mean of the horizontal and vertical velocities u' and w' can be further decomposed, giving turbulent quantities that are coherent with the surface waves $\tilde{u}$ and $\tilde{w}$. Hence, from the surface to a region significantly outside the viscous layer but close enough to the surface to be influenced by the waves, a fraction of the total stress is carried by the waves. Equation (1) is thus further decomposed, and the stress can be expressed as

$$\tau = \rho_a(\overline{u''w''} + \overline{\tilde{u}\tilde{w}} + \nu\overline{u}_z), \quad (4)$$

where the first term represents the turbulent stress, the second term is the stress carried by the waves, or form drag, and the last term is the molecular viscous contribution.

Over the last decade or so it has become apparent that surface wave processes can play an important role in the kinematics and dynamics of the boundary layers (e.g., Janssen 1989, 1999; Komen et al. 1994; Belcher and Hunt 1998; Hristov et al. 1998; Edson and Fairall 1998). Attention has been devoted to studying the stress carried by the waves, especially as it relates to the calculation of the fluxes using the bulk formula $u_*^2 = C_D(U_{10} - U_0)^2$, where U_0 is the velocity at the surface, or the surface current. Indeed, recent measurements and models of the drag of the sea surface on the atmosphere at moderate to high wind speeds suggest that much of the momentum transfer at the surface is supported by the form drag on the sea surface, which may be further resolved into a component that leads to wave growth and another component associated with flow separation over breaking waves (Kudryavtsev and Makin 2001; Makin and Kudryavtsev 2002; Donelan et al. 2004). Thus the waves are central to improved models of momentum transfer between the atmosphere and the ocean. In the late 1990s, following extensive study of the significance of the waves on the drag coefficient, the European Centre for Medium-Range Weather Forecasts (ECMWF) included wave effects in its parameterization of the air–sea drag coefficient in its coupled general circulation modeling.

With the recent interest in air–sea heat fluxes and satellite sea surface temperature (SST) measurements in the context of global climate change, including changes in hurricane intensity and frequency, there has also been a renewed interest in the thermal boundary layer at the ocean surface. However, there has been little interest in the potential influence of the surface waves on the heat and moisture fluxes. In fact, the role of surface waves in modulating heat transfer remains controversial at best, with some authors claiming that the waves play no direct role (Makin et al. 1995), while others argue that there is a possible influence, as the waves modulate eddy diffusivities (Makin and Mastenbroek 1996; Edson et al. 2004). Some argue that because there is no equivalent to the form drag (which is related to surface wave kinematics and dynamics) in the equations for the heat transfer, there is no significant influence of the waves on the heat transfer. On the other hand, the heat transfer clearly depends on the turbulent field, which may in turn be modulated by the waves (Belcher and Hunt 1998; Sullivan and McWilliams 2002). In a large-eddy simulation (LES), the latter authors found that the wave-induced heat flux

contributed as much as 15% of the total heat flux. Previous laboratory and field measurements of the temperature at (or near) the surface and the wave field have clearly showed some evidence of a finite correlation, but little attention has been paid to the consequences of these measurements for the air–sea heat transfer. In particular, authors have concentrated on correlating the surface temperature with η, the surface displacement, rather than with w, the vertical velocity. But it is the covariance of the temperature and velocity that is proportional to the sensible heat flux.

The literature on the modulation of the sea surface temperature by surface waves finds its roots in the study of the surface temperature and the cool skin (Ewing and McAlister 1960; McAlister 1964; Saunders 1967; also see the review by Katsaros 1980). As for the modulation of the surface (skin) temperature by the waves, to our knowledge the literature starts with O'Brien (1967), who studied the heat flux through a wavy surface from a Lagrangian frame and predicted, at most, a doubling of the heat flux. Later, Witting (1971, 1972) looked at the influence of progressive plane waves on the structure of the thermal boundary layer. Fixing the temperature gradient across the surface, he concluded that the heat flux could be increased by as much as a factor of 9 in the presence of highly nonlinear capillary waves. He also found that in the case of a cool skin, the surface temperature maximum leads the surface elevation maximum by $\pi/4$. Although Witting did not present his results in this context, the phase difference means that the covariance between the surface elevation (or orbital velocity) and the temperature is not zero.

The theoretical work of O'Brien (1967) and Witting (1971, 1972) motivated experimental laboratory work by Chang and Wagner (1975), who measured the magnitude of the surface temperature fluctuation induced by surface waves and found it was related to the magnitude of the heat flux. Later, Miller and Street (1978) found results in agreement with Witting's work for low wind speed, but observed departures from the theory at higher wind speeds. Witting's theory does not account for the wind; therefore agreement was not to be expected at any significant wind speed. One interesting result from Miller and Street's experiment is that the phase difference between elevation and temperature waves changed with the surface stress. They found that the maximum for the temperature wave moves from downwind to upwind of the elevation wave as the wind speed increases.

Simpson and Paulson (1980) performed a field experiment from the R/P *Floating Instrument Platform* (*FLIP*) and found that temperature waves exist at the surface of the ocean. They also observed, albeit over a limited wind speed range, that the maximum temperature was systematically upwind of the crest of the dominant waves. They concluded that the increased temperature was due to the thinning of the thermal boundary layer by the wind-induced stress. Jessup and Hesany's (1996) observations from R/P *FLIP* showed significant modulation of the surface skin temperature by swell. They found that the phase relationship between elevation and temperature waves depends on the relative direction between wind and swell. Interestingly, their data show the maximum temperature downwind of the dominant waves. They hypothesized that the temperature maximum is due to the presence of small-scale breaking waves induced by the modulation by the swell, which results in mixing and disruption of the surface skin layer. While the results of Jessup and Hesany (1996) agree with those of Simpson and Paulson (1980) and Miller and Street (1978) at a low wind speed, they did not observe a maximum in temperature on the upwind side of the waves at a higher wind speed. This difference has yet to be resolved. One significant difference between the experiment of Jessup and Hesany (1996) and others is the presence of very large swells. The resulting large wave age could explain why the thermal boundary layer on the upwind side could be less affected by the stress than it would be on the downwind side by the microscale breaking waves. Jessup has subsequently observed a phase relationship between temperature and elevation that is in accord with other experimental results (A. T. Jessup 2005, personal communication).

The LES modeling of Sullivan and McWilliams (2002) is particularly relevant to the role of wave-induced heat flux and its relationship to the wave-induced momentum flux. While their simulations are not directly relevant to the wave-induced temperature field at the surface (which they hold constant), they do show that the wave-induced heat transfer above the surface varies over a scale of $kz = O(1)$ (where k is the surface wavenumber) and may reach values of approximately 15% of the total sensible heat flux based on the air–sea temperature difference. They find that it can change signs in the neighborhood of the critical layer. In fact, they conclude that their proposed mechanism "for the organization of the temperature field in flow over waves is closely linked to the presence of a wave-induced velocity field."

We present results from three different field experiments and show evidence of temperature fluctuations $\tilde{T}$ that are coherent with the surface displacement due to the waves with a phase relationship that potentially leads to a sensible heat flux. We also use wave-modu-

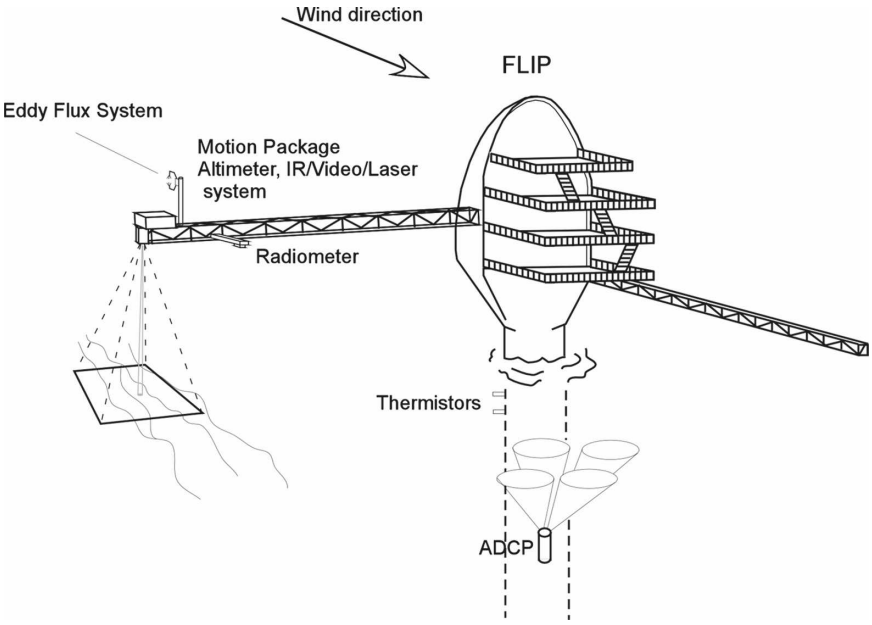

FIG. 1. Experimental setup on R/P *FLIP*.

lated temperature and humidity to estimate the corresponding wave-coherent latent heat flux obtained through eddy-correlation measurements at $O(10)$ m above the surface. We find that the fractional heat flux at $O(10)$ m above the surface, which can be attributed to wave-coherent processes, is in the range of 1%–10%, consistent with simple arguments suggesting that wave-induced scalar fluxes contribute a factor of $O(ak)^2$ to the total flux. While not a focus of this work, coincident measurements of the fractional wave-coherent momentum and CO_2 fluxes were found to be comparable to the fractional heat flux.

2. Experiments

The measurements described here were obtained from three different field experiments. The first was conducted from R/P *FLIP* when it was moored approximately 50 miles off the coast of San Diego, California (32°38.43′N, 117°57.42′W, 302 m deep), during 21–29 July 2002. A second was from R/P *FLIP* when it was moored west of Tanner Bank, California (32°40.20′N, 119°19.46′W, 312 m deep), during 20–26 August 2003. We also deployed the full system from Scripps Pier in a reduced-acquisition mode (two 20-min records per day), for a period of approximately 4 months from 4 December 2003 to 6 April 2004.

The main instruments comprised an active and passive infrared imaging and altimetry system (Veron et al. 2008) and a direct eddy covariance atmospheric flux package. Both systems are described in more detail below. From R/P *FLIP*, instruments were deployed at the end of the port boom (Fig. 1) approximately 18 m from the hull at an elevation of 13 m above mean sea level (MSL). Additional supporting data were obtained from a Workhorse Waves ADCP (Teledyne RDI, 600 kHz, at a depth of 15 m on the hull of R/P *FLIP*), which yielded directional wave spectra and significant wave heights for the duration of the experiment; two subsurface fast-response thermistors (Branker TR-1040, 95 ms) placed on the hull of R/P *FLIP* at 2- and 1.2-m depths; GPS position and R/P *FLIP* heading. The same eddy covariance and infrared packages were deployed from a boom at the end of Scripps Pier approximately 10 m out from the pier deck, at an elevation of 14 m above MSL. Subsurface temperature and supporting meteorological data were also available from the Scripps Pier meteorological station (CDIP 073), and incident wave conditions were provided by an RDI Waves ADCP seaward of the pier (available online at http://cdip.ucsd.edu).[1]

a. Infrared imaging and altimetry system

The active and passive infrared imaging and altimetry system includes an infrared camera (Amber Galileo), a 60-W air-cooled CO_2 laser (Synrad Firestar T60) equipped with an industrial marking head (Synrad

[1] CDIP 073 refers to the Scripps Pier site in the Coastal Data Information Program.

FH index) with two computer-controlled galvanometers, a laser altimeter (Riegl LD90–3100-EHS), a video camera (Pulnix TM-9701), a 6-degree-of-freedom motion package (Watson Gyro E604), and a single-board computer (PC Pentium 4). All instruments were enclosed in a weatherproof, air-conditioned aluminum housing. All instruments and computers were synchronized to within 2 ms and also to GPS time. The infrared camera was set to record temperature images (256 × 256 pixels) at 60 Hz, with a 2-ms integration time, yielding better than a 15-mK resolution. We note here that the infrared imager was calibrated pre- and postdeployment and that temperature nonuniformity corrections were performed at sea using a uniform temperature target. The nonuniformity calibration was performed once the camera had reached its operating temperature, and the camera was not powered down for the remainder of the experiment. While the slope of the calibration curve (linear in the range of temperature encountered here: $r^2 = 0.999\,26$) is sufficiently stable to afford the repeatable relative temperature resolution quoted above; in our case, the absolute temperature measurement could only be achieved to within 400 mK. This was confirmed with a comparison between the sub–skin temperature measurement estimated from the infrared camera and the highest subsurface thermistor measurement. Both measurements agreed within the estimated 400-mK accuracy. The absolute accuracy of the system could be improved upon by using a blackbody and frequent calibrations. Accordingly, the results and techniques presented here only rely on accurate relative temperature measurements. Calibrations and nonuniformity corrections were performed with the optical window in place to account for its effects. Reflections from the boom were sometimes observed in the datasets at the lowest wind speeds (less than 2–3 m s^{-1}). These data were ignored in the subsequent analysis. The video camera (768 × 484 pixels) was synchronized to the infrared camera and acquired full frames at 30 Hz. The infrared CO_2 laser and accompanying marking head were used to actively lay down patterns of thermal markers on the ocean surface to study the rate of decay of an imposed surface temperature perturbation while tracking the Lagrangian velocity, shear, and vorticity at the surface. The detailed performance of the passive and active IR measurement system for ocean-surface kinematics is the subject of a separate publication (Veron et al. 2008). Finally, the laser altimeter measured the distance to the water surface within both the infrared and video images, at 12 kHz (averaged down to 50 Hz) with a footprint of 5 cm in diameter. For the R/P *FLIP* experiments, infrared and video images were acquired for 20 min every hour, with supporting data acquired continuously for the duration of the experiments. Figure 2 shows examples of sea surface temperature images taken from R/P *FLIP* in July 2002. The images show significant structure in the surface temperature field, albeit within a small overall temperature range. The position of the footprint of the laser altimeter is indicated here by the white disk near the center of the image. In the results section, correlations between surface temperature and surface displacement are made at the location of the footprint of the laser altimeter.

b. *Eddy covariance system*

In addition to the optical infrared system, we used an eddy covariance system to acquire supporting meteorological and boundary layer flux data. The eddy covariance system included a three-axis anemometer/thermometer (Campbell CSAT 3), an open-path infrared hygrometer/CO_2 sensor (Licor 7500), a relative humidity/temperature sensor (Vaisala HMP45), and a net radiometer (CNR1). The sonic velocity was corrected to account for the motion of R/P *FLIP* using the acceleration measurements obtained with the motion package (Edson et al. 1998). The sonic temperature was corrected for humidity and pressure, and the latent heat flux was corrected for density variations (Webb et al. 1980). The velocity was then projected into a frame of reference aligned with the mean wind direction, and the turbulent fluxes of momentum, heat, and moisture were calculated over 30-min averages. Figure 3 shows a comparison between the fluxes measured with the eddy-covariance system and those calculated with bulk formulas from the Tropical Ocean and Global Atmosphere Coupled Ocean–Atmosphere Response Experiment (TOGA COARE) 3.0 algorithm (Fairall et al. 1996, 2003), for the data of the August 2003 experiment. For the most part, the agreement is good and supports the use of the Monin–Obukhov similarity theory for open-ocean conditions (Edson et al. 2004). However, there are significant differences in the sensible heat flux toward the end of the experiment, with the TOGA COARE algorithm giving fluxes up to 30% less than those measured. Also, the algorithm does not reproduce the short-term fluctuations in any of the fluxes, although this should be expected for any empirical algorithm based on a "best fit" to the data. Similar agreement (not shown) was obtained at Scripps Pier. The eddy covariance system was not deployed during the first R/P *FLIP* experiment in 2002. For the purposes of this paper, the generally good agreement gave us confidence that our covariance measurements were consistent with other measurements in the litera-

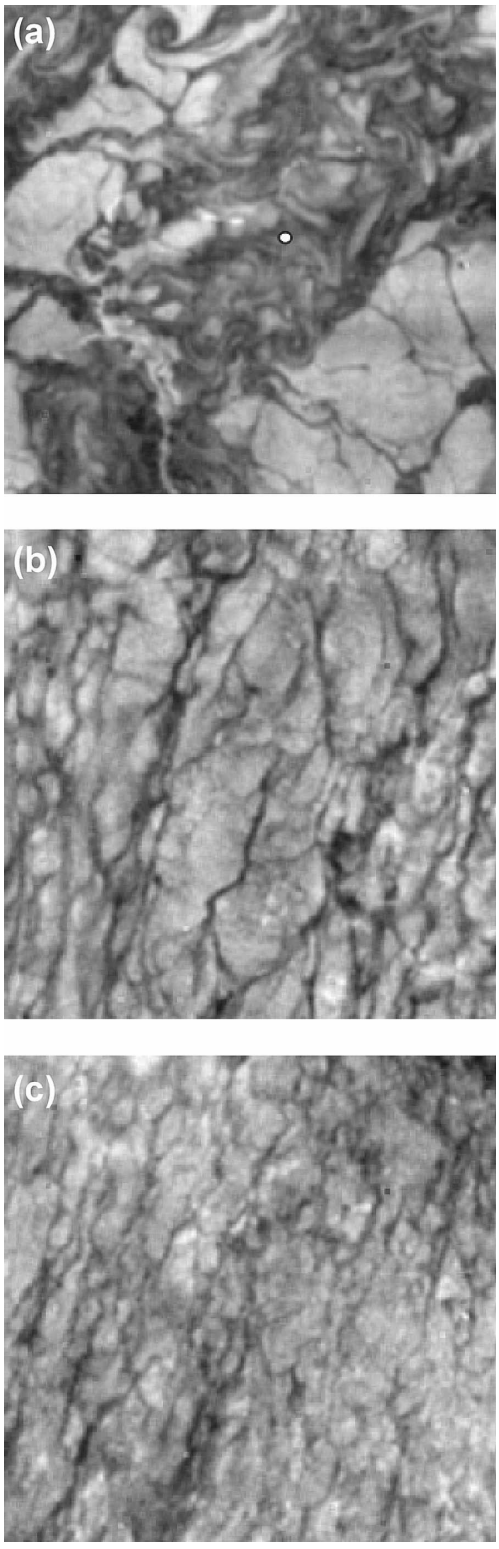

FIG. 2. Surface temperature images taken from R/P *FLIP* at wind speeds of (a) 0.1, (b) 0.9, and (c) 2.4 m s^{-1}, respectively. The white disk shows the location of the footprint of the laser altimeter. The grayscale indicates surface temperature; light gray is warmer and dark gray is colder. Note the qualitative change in the structure of the temperature field with increasing wind speed.

ture of the total flux above the diffusive and wave boundary layers.

3. Wave-induced heat flux

a. Surface fluxes

Before presenting the measurements, it is useful to consider a simple treatment of the heat (or other passive scalar) transfer across the surface in the presence of steady surface waves. We consider steady two-dimensional waves, uniform in the y direction, propagating in the x direction over water infinitely deep. We denote the temperature of the water by T.

Using the subscript notation for differentiation, the heat equation is

$$T_t + (uT)_x + (wT)_z = \kappa_w(T_{xx} + T_{zz}), \tag{5}$$

where κ_w is the thermal diffusivity in water.

The sea surface, $z = \eta(x)$, is steady in a frame of reference moving with the wave-phase speed c and has a wavelength of λ. Denoting the integral from $-\infty$ to the surface, $\eta(x)$, by

$$\int_{-\infty}^{\eta(x)} \ldots dz = \langle \ldots \rangle, \tag{6}$$

integrating the heat equation, and using the Leibniz rule, we get

$$\langle T\rangle_t + \langle uT\rangle_x - (uT)|_\eta \eta_x + (wT)|_{-\infty}^{\eta} = \langle \kappa_w T_x\rangle_x - \kappa_w T_x|_\eta \eta_x + \kappa_w T_z|_{-\infty}^{\eta}. \tag{7}$$

Applying the conditions at $z = \eta$ and $-\infty$, this becomes

$$\langle T\rangle_t + \langle uT\rangle_x - (uT)|_\eta \eta_x + (wT)|_\eta = \langle \kappa_w T_x\rangle_x - \kappa_w T_x|_\eta \eta_x + \kappa_w T_z|_\eta. \tag{8}$$

Now the kinematic condition at $z = \eta(x)$ is

$$u\eta_x = w. \tag{9}$$

Therefore,

$$-(uT)|_\eta \eta_x + (wT)|_\eta = 0, \tag{10}$$

and the integrated heat equation further simplifies to

$$\langle T\rangle_t + \langle uT\rangle_x = \langle \kappa_w T_x\rangle_x - \kappa_w T_x|_\eta \eta_x + \kappa_w T_z|_\eta. \tag{11}$$

Denoting the horizontal average over one wavelength by the overbar and multiplying by $\rho_w C_{pw}$, we are given the rate of change of heat content per unit area of ocean surface, or the heat flux *into* the ocean surface Qs, by

$$\mathrm{Qs} \equiv \rho_w C_{pw} \overline{\langle T\rangle}_t = \rho_w C_{pw} \kappa_w (-\overline{T_x|_\eta \eta_x} + \overline{T_z}|_\eta). \tag{12}$$

In the absence of surface waves, η_x is zero, the first term on the right-hand side of Eq. (12) is zero, and the

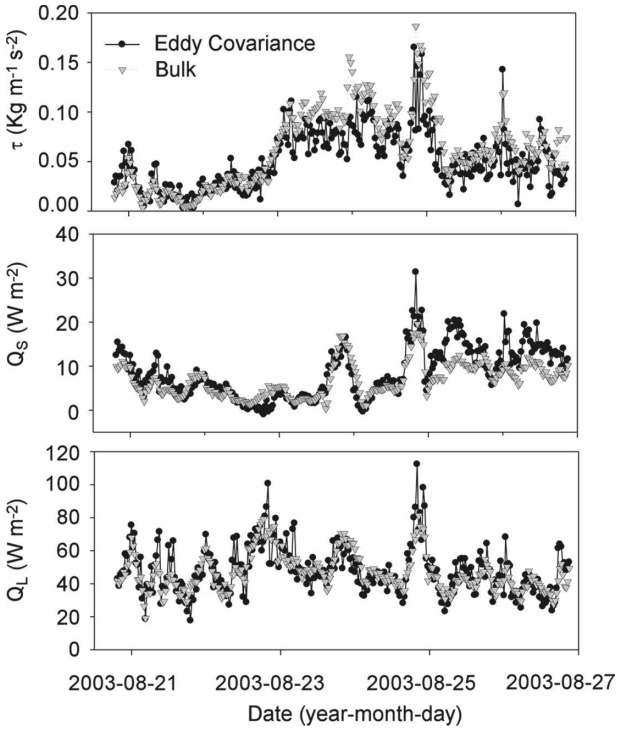

FIG. 3. Surface stress, heat, and moisture fluxes measured by the eddy covariance system compared to the TOGA COARE 3.0 bulk algorithm for the 2003 experiment.

usual vertical gradient diffusion of heat at the horizontal interface is given by the second term. With waves, η_x is nonzero, and the first term on the right-hand side contributes explicitly to the heat flux while the second term may contribute implicitly because of straining of the fluid by the waves and therefore the vertical gradient in temperature. In many cases there will be a thin—O(mm)—thermal diffusive boundary layer at the surface of thickness $\delta_T \ll \lambda$, where λ is the surface wavelength. If this boundary layer is locally of uniform thickness parallel to the surface, then $T_x = -T_z\eta_x$, and, to leading order, the heat flux is given by

$$\begin{aligned} \mathrm{Qs} &\approx \rho_w C_{pw}\kappa_w \overline{T_z|_\eta(1 + \eta_x{}^2)} \\ &= \rho_w C_{pw}\kappa_w \overline{T_z}|_\eta \left[1 + \overline{\eta_x^2} + \frac{\overline{T_z'|_\eta(\eta_x^2)'}}{\overline{T_z}|_\eta}\right], \end{aligned} \quad (13)$$

where the prime denotes the departures from the horizontal average. The last term in brackets is at most $O(ak)^3$ and can be neglected compared to $\overline{\eta_x^2}$. Earlier theoretical studies of wave-modulated heat flux in the absence of wind forcing (Witting 1971) have shown that the presence of gravity waves may augment the heat flux by a factor of $1 + O(a^2k^2)$, where $ak \ll 1$ is the wave slope. For Stokes limiting waves the heat transfer was augmented by a factor of 1.38. Witting also found that steady capillary waves may augment the heat flux by as much as an order of magnitude for negligibly thin thermal boundary layers, although the application of steady capillary wave theory to oceanic conditions may be tenuous. Nevertheless, even an increase by a factor of $O(a^2k^2)$ is significant when wave slopes ak may range up to approximately 0.3 (Melville 1996), giving a potential increase in heat transfer of up to $O(10\%)$.

b. Fluxes in the marine atmospheric boundary layer

As in Eq. (4), fluctuations of the temperature θ' and the water vapor q' can be resolved into wave-coherent (indicated by a tilde overbar) and turbulent parts (indicated by a double prime),

$$\theta' = \tilde{\theta} + \theta'' \quad \text{and} \quad (14)$$

$$q' = \tilde{q} + q'', \quad (15)$$

and substituting into Eqs. (2) and (3) gives

$$\mathrm{Qs} = \rho_a C_{pa}(\overline{\theta''w''} + \overline{\tilde{\theta}\tilde{w}} + \kappa_a\overline{\theta}_z) \quad \text{and} \quad (16)$$

$$\mathrm{Ql} = \rho_a L_v(\overline{q''w''} + \overline{\tilde{q}\tilde{w}} + D\overline{q}_z), \quad (17)$$

where cross terms make no contribution to the averages.

The eddy flux measurements of sensible and latent heat presented below were made at elevations of $O(10)$ m in the MABL, by which point we expect the wave-coherent and turbulent terms to far exceed the molecular terms. While wave-induced flux contributions may be inferred from parameterizations that include surface wave parameters, such methods are indirect and have not been evaluated in the latest bulk parameterizations of air–sea fluxes (Fairall et al. 2003). We wish to directly measure terms of the form $\overline{\tilde{\theta}\tilde{w}}$, by separating the wave-coherent contribution to the covariance of the fluctuations from the turbulent contributions. As far as we are aware, there are no general techniques for separating wave-induced fields from turbulence, especially in field measurements. After trying various methods on the data, including the phase-averaging technique of Hristov et al. (1998), which appeared to produce inconclusive results for our data, we found that linear transform techniques gave consistent and seemingly conservative estimates of the wave-coherent fluxes. We used the coherence and phase of each variable with the surface displacement η by the waves immediately below the atmospheric measurements. By denoting the squared coherence of w' and η in the frequency domain by $C_{w\eta}$, the phase by $\Phi_{w\eta}$, and the spectrum of w' by S_{ww}, then the spectrum of w' coherent with the waves (i.e., the spectrum of $\tilde{w}$) is given by $S_{\tilde{w}\tilde{w}} = S_{ww} \times C_{w\eta}$.

Similarly, the spectrum of $\tilde{\theta}$ is given by $S_{\tilde{\theta}\tilde{\theta}} = S_{\theta\theta} \times C_{\theta\eta}$, and the corresponding phase is $\Phi_{\theta\eta}$. It follows that the covariance of the wave-modulated temperature and vertical velocity $\overline{\tilde{w}\tilde{\theta}}$ is given by

$$\overline{\tilde{w}\tilde{\theta}} = \int (S_{\tilde{w}\tilde{w}} S_{\tilde{\theta}\tilde{\theta}})^{1/2} \cos(\Phi_{w\eta} - \Phi_{\theta\eta})\, d\omega, \qquad (18)$$

where the integral is over the bandwidth of the surface gravity wave field.

We expect these estimates to be conservative since the wave-modulated heat flux will eventually decay with vertical distance from the surface. There is also the issue of horizontal decorrelation between variables measured above the surface and those at the surface. This occurs because atmospheric variables measured at elevation have a Lagrangian trajectory that goes back in time to a location at the surface upstream of the point of measurement. We can make a crude estimate of this distance and the time taken using a simple result for the mean Lagrangian transport of a passive scalar in a logarithmic boundary layer for which the mean velocity is given by $U(z)/u_* = \ln(z/z_0)/\kappa$. Since u_* is the only velocity scale, the mean Lagrangian velocity is simply $O(u_*)$ away from the surface. Thus the time to travel from the surface to a height $z = Z$ is $T = Z/u_*$. The distance traveled in that time $X(T)$ is simply

$$X(T) = \frac{u_*}{z_0} \int_0^T \ln\left[\frac{z(t)}{z_0}\right] dt, \qquad (19)$$

$$= \frac{z_0}{\kappa}\left[\frac{Z}{z_o}\ln\left(\frac{Z}{z_o}\right) - \frac{Z}{z_o} - 1\right], \qquad (20)$$

where we have taken the surface to be at $z = z_0$ ($z' = 1$).

If $Z/z_0 \gg 1$, then to a good approximation

$$X(T) \approx \frac{Z}{\kappa}\left[\ln\left(\frac{Z}{z_0}\right) - 1\right], \qquad (21)$$

$$= C_{DZ}^{-1/2} Z, \qquad (22)$$

where C_{DZ}, the drag coefficient evaluated at a height of Z, is $O(10^{-3})$ for $Z = O(10)$ m. This estimate suggests that passive scalars and perhaps, to a leading order, vorticity perturbations at the surface will travel distances of $O(100)$ m downwind before reaching an elevation of $O(10)$ m. We further need to estimate to what extent the wave field decorrelates as the waves travel downwind for such distances. If a particular wave of wavelength λ originating at X m upwind of the sensor travels with a phase speed of c, it will reach the sensor in a time of X/c. To retain significant correlation, we can, for example, require that the wave remains within a wave group traveling with the group velocity of c_g. Let us assume that there are approximately $n = O(10)$ waves in a group and that a wave travels no farther than half the length of the wave group ($n\lambda/2$) while it propagates toward the sensor. In other words, we are assuming that at least half the waves present in the group at a distance of X from the sensor remain present directly beneath the sensor. In deep water, this leads to the constraint on the wavelength that $X/c \le \lambda n/2c_g = \lambda n/c$. From here, we estimate the maximum frequency f_m at which we anticipate observing a correlation as a function of the wind speed (drag coefficient) and a given measurement height:

$$f_m = \sqrt{\frac{ngC_{DZ}^{1/2}}{2Z\pi}}. \qquad (23)$$

We then compare the maximum frequency f_m for which we expect to be able to observe a correlation at height Z with the peak wave frequency that we observe; it is then deduced that in deep water we do not expect to see wave-coherent contributions to these flux measurements at 10 m for wind speeds lower than approximately 5 m s^{-1}. In shallow water, the phase and group velocity are the same and we do not expect significant decorrelation of the wave field over a distance of $O(100)$ m, even at very low wind speeds.

The measurements described below demonstrate that there is a wave-coherent contribution to the surface temperature and a wave-coherent contribution to sensible and latent heat fluxes measured at distances of $O(10)$ m above the ocean surface.

4. Results

As described above, the footprint of the laser altimeter was located within the infrared image. This also allowed us to examine the modulation of the surface temperature by the waves. From the infrared images, we have generated time series of the temperature averaged over the footprint of the altimeter. To avoid sky reflectance and other effects, only nighttime temperature time series were used. Longwave downwelling and upwelling measurements also indicate that contamination by "warm" clouds is negligible. We have made sure that no contamination by the active IR spot was present. Figure 4a shows time series of surface temperature T and the surface displacement η over a 50-s record starting at 0900 UTC 25 August 2003. There is a clear visual correlation between the two variables. Frequency spectra of η and T, $S_{\eta\eta}$ and S_{TT}, respectively, over a 20-min record beginning at 0900 UTC 25 August 2003 are shown in Fig. 4b. The quality of the near–IR laser wave-gauge data is dependent on the roughness of the sea surface with dropouts increasing for lower wind

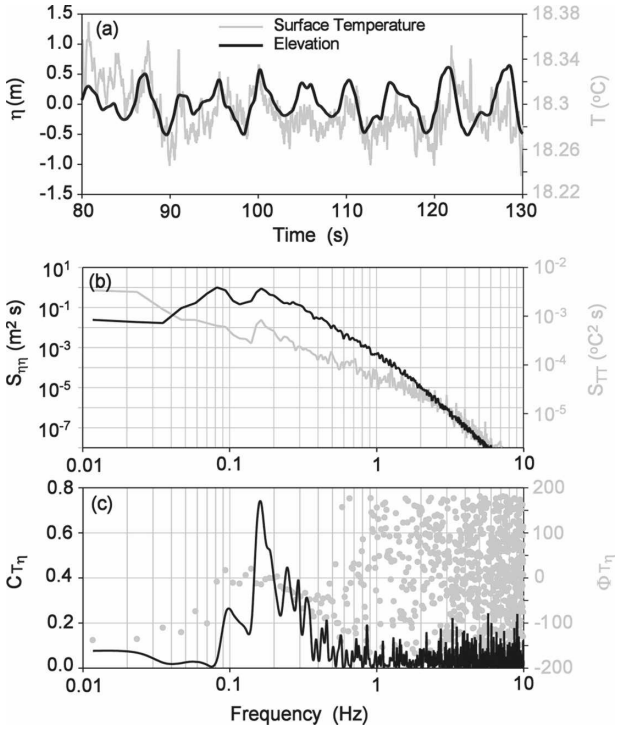

FIG. 4. (a) Time series of surface temperature and displacement over a 50-s record starting at 0900 UTC 25 Aug 2003, showing the clear correlation between the two time series. (b) Spectra of surface temperature and displacement for a 20-min record starting at 0900 UTC 25 Aug 2003, showing clear wind-wave peaks in both spectra and a more prominent swell peak in the wave record. (c) The corresponding squared coherence and phase between the two time series showing the strong coherence at the wind-wave peak, although a weaker peak is also apparent in the band of swell frequencies.

speeds. The data shown here were good for frequencies of up to 1 Hz and were low-pass filtered at that frequency. The surface-displacement spectrum is unremarkable, showing both wind-wave and swell peaks at 0.16 and 0.08 Hz, respectively, and a ω^{-4} slope above the wind-wave peak. The temperature data are considered accurate for the full range of frequencies shown—up to 10 Hz. The temperature spectrum displays a peak at the wind-wave peak frequency and a ω^{-1} slope above the wind-wave peak up to 2–3 Hz, and then $\omega^{-9/2}$ up to 10 Hz. There is some hint of a local maximum around the frequency of the swell, but this is masked by the trend toward a "red" spectrum at the lower frequencies. Figure 4c shows the squared coherence and phase with a peak in the squared coherence of 0.74 at the wind-wave peak and a much lower peak of approximately 0.3 at the swell frequencies. The phase in the neighborhood of these peaks is in the range of $\pm\pi/8$. The phase difference at the wind-wave peak shows the wind waves leading the temperature waves by 10°–20°. In the rest of the text, a negative phase indicates that the peak temperature lags the peak elevation; that is, the peak temperature is situated on the windward side of the surface wave. A phase equal to 0 indicates that both the temperature and the elevation maxima are congruent.

Figure 5a shows frequency spectrograms of the surface displacement for the duration of the R/P *FLIP* experiment in August 2003. The swell peak is clear, and also a wind-wave peak appears with the wind event (Fig. 5e), showing the classical downshift in wind-wave peak frequency with time. Figure 5b shows that the frequency spectra for the temperature exhibit peaks at the local maxima of the wind-wave spectra. Less apparent but nonetheless present are maxima in the temperature spectra at the swell-peak frequencies. Figures 5c,d show that the low-frequency long waves (swell and wind waves) correlate well with the temperature fluctuations, while the coherence rapidly goes to zero at frequencies above approximately 1 Hz. The phase between the temperature and the surface displacement near the peak of the coherence is negative, indicating that the maximum in temperature lags the maximum surface displacement. These results are qualitatively consistent with the results of Simpson and Paulson (1980) and Miller and Street (1978), but depart from those of Jessup and Hesany (1996), at least at the higher wind speeds. The reason for this discrepancy is still unclear, but more recent measurements by A. T. Jessup (2005, personal communication) are consistent with our results and others cited herein. While we find that the phase between surface displacement and temperature waves at the surface is negative, it shows a trend with the wind speed.

We have taken the phase differences between surface displacement and temperature at the wave-peak frequency (both swell and wind waves when two peaks were present) and plotted them in Fig. 6 as a function of wind speed for all three experiments. We only show the phase for which the coherence was larger than 0.3 (a significant correlation given sampling rate and window sizes). The phase lag exhibits a variation as a function of wind speed similar to that observed in the laboratory by Miller and Street (1978). The large gray circle at zero wind speed corresponds to the theoretical results of Witting (1972). A negative phase indicates that the temperature peak lags the surface wave peak. The scatter in the data also suggests that perhaps some other parameter, such as wind direction relative to the wave direction as suggested by Jessup and Hesany (1996), could play an important role (e.g., see the outliers from the experiment on Scripps Pier). The large white sym-

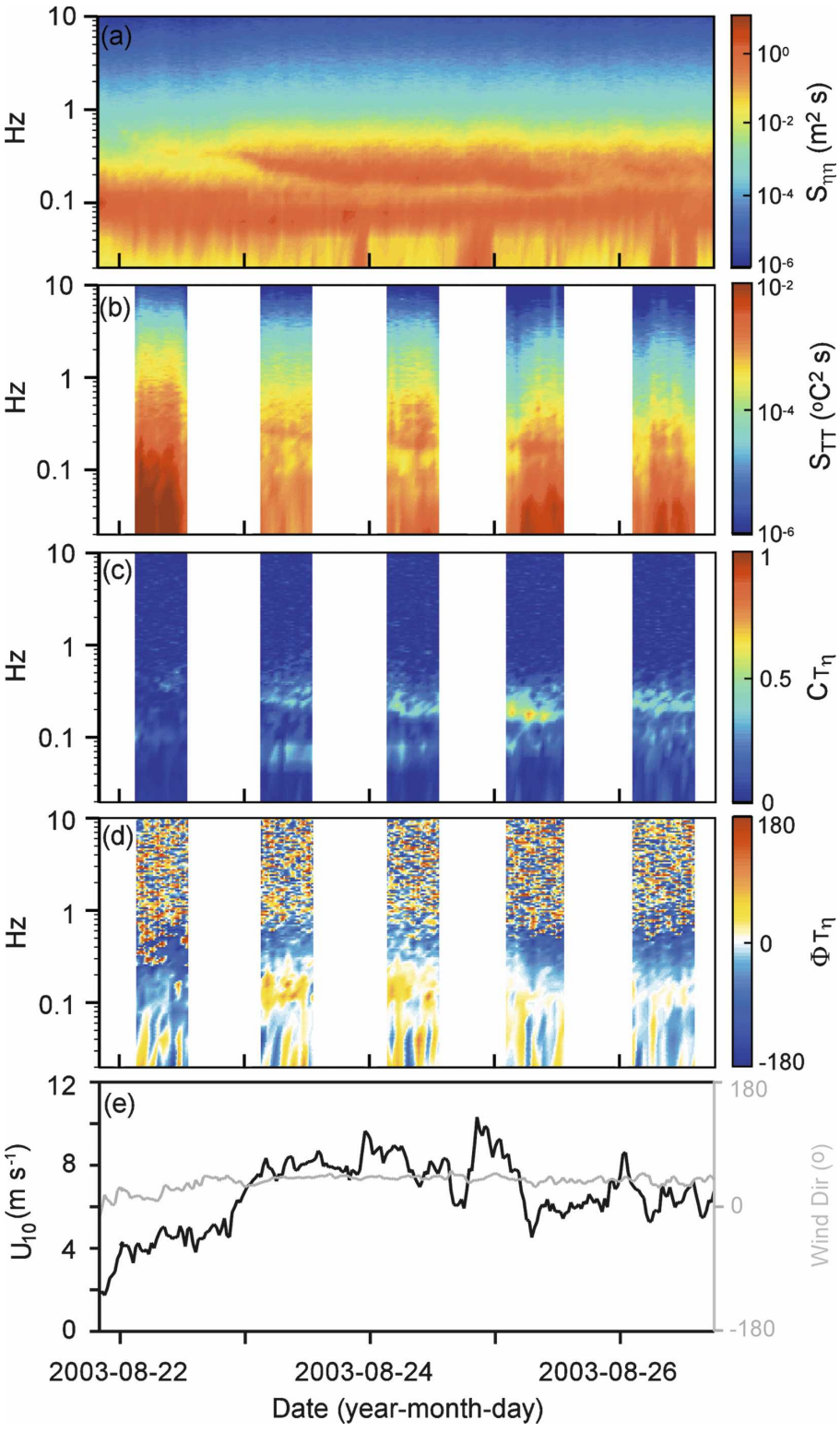

FIG. 5. Spectrograms of (a) the surface displacement and (b) the surface temperature at night for the 2003 experiment. (c),(d) The squared coherence and phase between the surface displacement and temperature, respectively. (e) Wind speed and direction for the duration of the experiment.

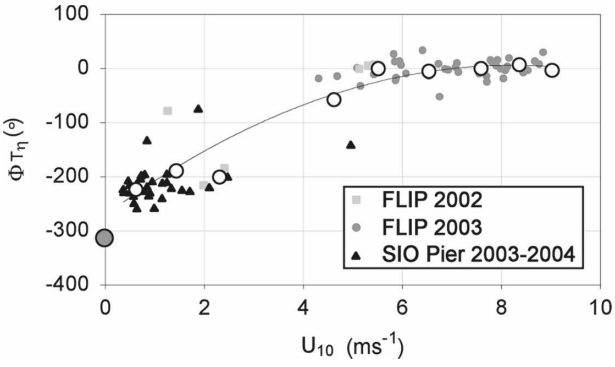

FIG. 6. Phase relationship between surface temperature and elevation as a function of wind speed. A negative phase indicates that the maximum temperature is upwind of the surface wave crest. The large gray symbol for $U_{10} = 0$ m s^{-1} shows the theoretical result of Witting (1972). Large white symbols are bin-averaged data. Note here that the phase is shown in the interval $[-2\pi, 0]$ instead of $[-\pi, \pi]$ to avoid wrapping and to illustrate the continuous phase shift with increasing wind speed.

bols are the bin-averaged data in increments of U_{10} of 1 m s^{-1}.

In the absence of direct measurements of the thermal boundary layers in the immediate neighborhood of the surface, we cannot use the surface temperature and surface displacement to directly measure the wave-modulated heat flux in Eq. (13); however, using the procedure outlined in section 3b we can estimate the wave-modulated heat flux in the atmospheric boundary layer at elevations of $O(10)$ m based on linear-coherence techniques.

Figure 7 shows the wave-coherent sensible, latent, and total heat fluxes for the duration of the 2003 R/P *FLIP* experiment, along with the significant wave height H_S and the wind speed at 10 m U_{10}. The data are shown for wind speeds larger than $U_{10} = 5$ m s^{-1}. The wave-coherent sensible and latent heat fluxes generally follow the trend of the wind and wave data, displaying local peaks corresponding to the wind and wave maxima within the noise of the data. The maximum wave-coherent sensible and latent heat fluxes were approximately 1 and 3.5 W m^{-2}, respectively, with the maximum in the total wave-coherent heat flux reaching 4 W m^{-2}.

Figures 8 and 9 show the wave-coherent sensible, latent, and total heat fluxes as a function of the 10-m wind speed U_{10} and the variance of the "slope"[2] of the wave field $(ak)^2$, respectively. The data are shown for

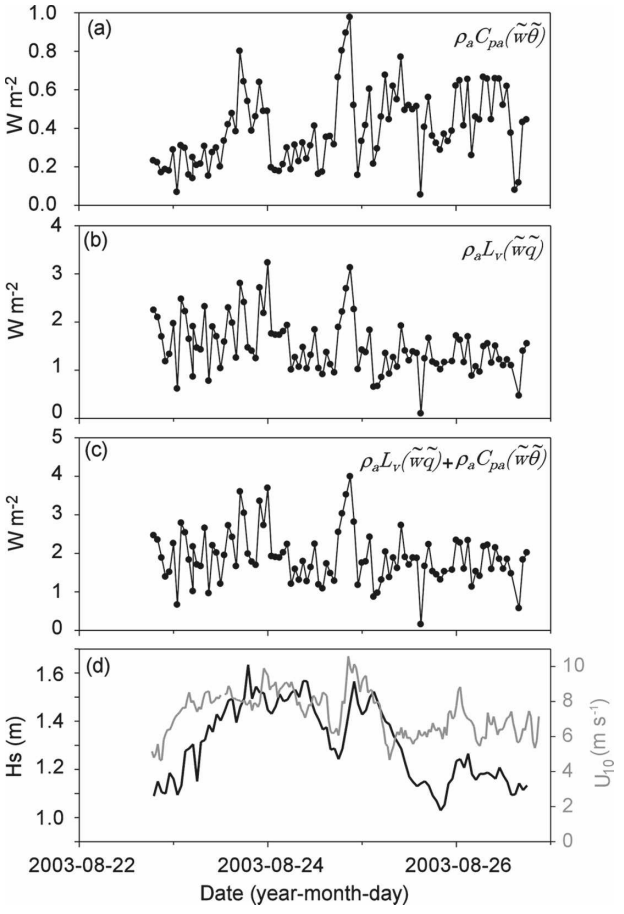

FIG. 7. Wave-coherent (a) sensible, (b) latent, and (c) total heat fluxes during the 2003 R/P *FLIP* experiment, along with U_{10} and (d) the significant wave height.

both the 2003 R/P *FLIP* experiment and the 2003–04 Scripps Pier experiment. The large gray dots show the bin-averaged data. There is clearly some correlation between the wave-coherent heat flux and the wind speed and also with the variance of the wave slope as suggested by the simple model in section 3a. There is, however, some significant scatter in the data that is most likely a consequence of the fact that the total (turbulent and wave coherent) fluxes of heat and water vapor are also dependent on the air–water temperature difference and atmospheric relative humidity. Therefore, while the absolute values of wave-coherent fluxes are of interest, especially with regard to other contributors to air–sea fluxes, our particular interest here is in isolating the wave effects. Hence, it is of more interest to consider the fraction of the total flux that can be attributed to surface wave effects, and so we compute the fractional contribution of the wave-coherent fluxes to the total fluxes. For example, $\tilde{w}\tilde{\theta}/\overline{w'\theta'}$ is the wave-

[2] Since the surface slope, (η_x, η_y), was not directly measured in the experiments, the variance of the slope is estimated from the wave-frequency spectrum, $S_{\eta\eta}$, by $\int_0^\infty S_{\eta\eta}\omega^4 g^{-2}\, d\omega$.

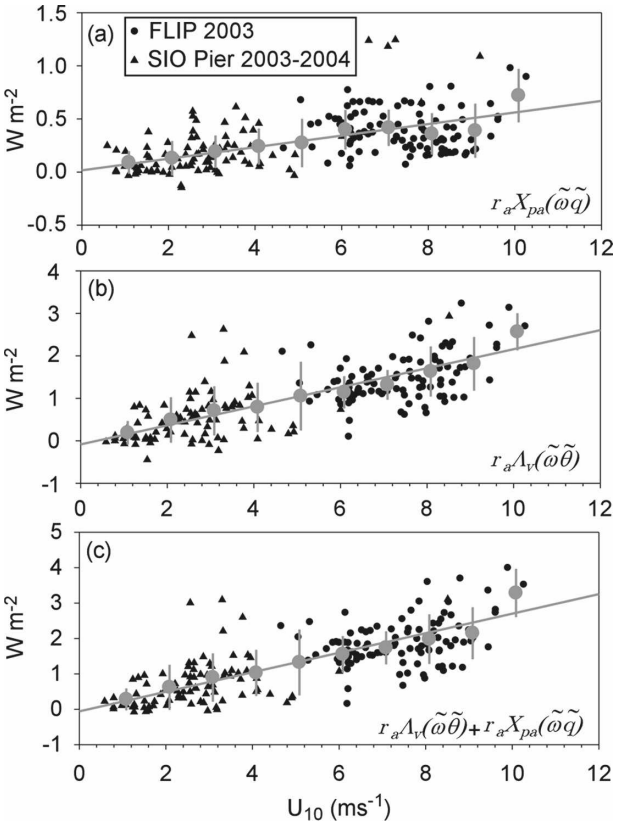

FIG. 8. Wave-coherent (a) sensible, (b) latent, and (c) total heat fluxes as a function of the 10-m wind speed for the 2003 R/P *FLIP* experiment (dots) and the 2003–04 SIO pier experiment (triangles). The large gray dots show the bin-averaged data.

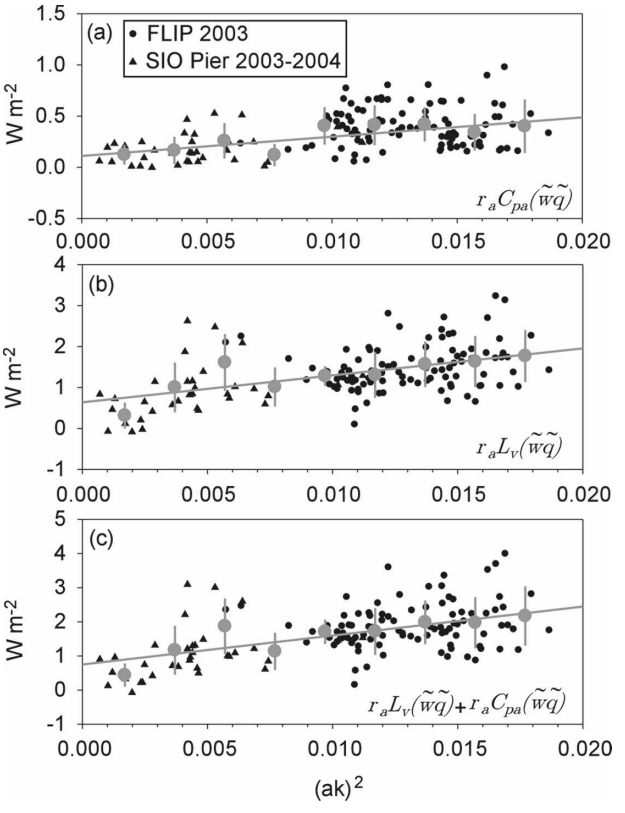

FIG. 9. Wave-coherent (a) sensible, (b) latent, (c) and total heat fluxes as a function of the variance of the surface wave slope for the 2003 R/P *FLIP* experiment (dots) and the 2003–04 SIO pier experiment (triangles). The large gray dots show the bin-averaged data.

coherent fraction of the sensible heat flux. This is, however, a delicate operation because the total turbulent fluxes become small at low wind speeds. Such fractional estimates will likely yield noisy results at low wind speeds.

Figure 10 illustrates the dependence of the fractional total heat flux on the variance of the slope for the 2003 R/P *FLIP* experiment and the 2003–04 Scripps Pier experiment. The maximum fraction of the sensible heat flux attributed to wave effects in these data is 15% (not shown) and the maximum fraction of the latent heat flux is approximately 7% (not shown), as is the fraction of the total heat flux, since the latent heat flux is generally much larger than the sensible heat flux. Despite the large scatter, the fractional data indicate some correlation between the wave-coherent heat flux and the variance of the wave slope, with the wave-coherent fraction of the flux of the same order of magnitude as the wave-slope variance. However, there is a lot of scatter in the data, implying other dependencies not considered here. Some may be from the z dependence of the wave-induced flux, which might contain both oscillatory and monotonically decaying components having a surface wavenumber dependence (cf. Sullivan and McWilliams 2002), whereas these measurements were made at a fixed height above MSL.

5. Discussion

Since the meteorological package was able to measure Reynolds stresses and CO_2 fluxes and since the simple wave-coherent flux-scaling model applies at least to scalar fluxes, including gases, we took the opportunity to show the corresponding wave-coherent momentum and CO_2 and fluxes for the same experiments as shown in Fig. 11. The data show that both the CO_2 and the momentum fluxes attributed to wave-coherent processes, like those for water vapor and heat, increase with wind speed. In fact, the fractional CO_2 and momentum fluxes are comparable to the heat flux fractions and of the order of the wave slope variance.

We have shown that a fraction of the total heat flux at the ocean surface is supported by the surface waves. The wave-coherent heat flux in field experiments that

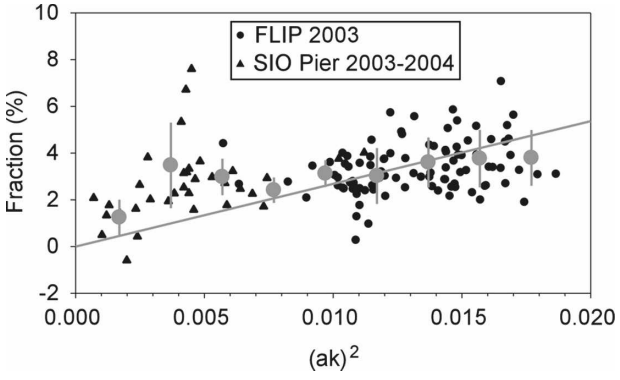

FIG. 10. The fraction of the total heat flux that is attributed to wave-coherent processes plotted against the variance of the surface slope during the 2003 R/P *FLIP* experiment and the 2003–04 SIO pier experiment. The large gray dots show the bin-averaged data.

span the global average wind speed is $O(1)$ W m^{-2}. We have also shown that the phase relationship between elevation and temperature waves depends on the wind speed. The peak in temperature is located on the rear face (upwind) of the surface waves (phase between $-180°$ and $0°$) for wind speeds larger than 1 to 2 m s^{-1}. This appears to agree with the suggestions of Simpson and Paulson (1980) that the increase in surface temperature was a result of the thinning of the thermal boundary layer by the wind stress on the rear face of waves. At very low wind speeds, the temperature peak is located on the front face (downwind) of the surface waves. This is consistent with the theoretical results of Witting (1972) and the laboratory data of Miller and Street (1978). The wind speed dependence of the phase is also in agreement with the laboratory data of Miller and Street (1978). At very low wind speeds, the modulation of the surface temperature is likely caused by the mechanical straining of the surface, inducing a peak temperature on the front face of the wave, while at higher wind speeds, the wind stress contributes to the thinning of the thermal boundary layer. At even higher wind speeds, microbreakers, parasitic capillary waves, and eventually larger breaking waves locally destroy the surface thermal diffusive layer, creating an enhanced surface temperature on the front face of the waves. This could in fact explain part of the data of Jessup and Hesany (1996), who found a positive phase between the surface waves and temperature fluctuations when the wind and waves were copropagating. Indeed, their data were collected at relatively low wind speeds ($U_{10} < 6$ m s^{-1}) in the presence of large swell. It is then possible that the temperature modulations that they observed were the result of mechanical straining. However, this does not explain their observations of the phase dependence on the relative direction of the wind and swell.

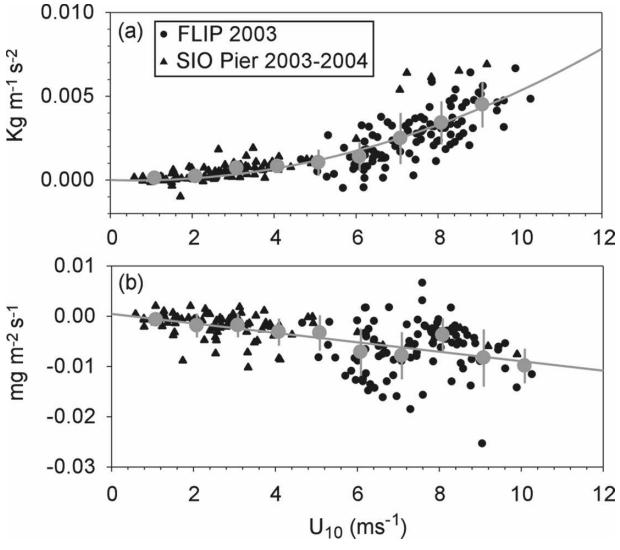

FIG. 11. The fluxes of (a) momentum and (b) CO_2 that are attributed to wave-coherent processes plotted against the wind speed during the 2003 R/P *FLIP* experiment. The large gray dots show the bin-averaged data.

We found that at $O(10)$ m above the MSL, the wave-coherent sensible heat flux was approximately 5%–15% of the total sensible heat flux in unstable atmospheric conditions. This compares favorably with the results of Sullivan and McWilliams (2002), who found in similar stability conditions that the wave-induced heat flux could be as much as 15% of the total heat flux. Their maximum contribution from the wave was located at the critical height, while they had a wave-coherent heat flux of zero at the surface because they imposed a constant surface temperature.

It is interesting to note that the dependences of the phase and wave height on the wind speed are competing with the effects in setting the value of the wave-coherent heat flux. As the wind speed increases, the wave-height variance increases. But with increasing wind speed, the phase between surface displacement and temperature fluctuations approaches zero (Fig. 6a), thereby diminishing the covariance between the surface temperature and the velocity, at least at the surface. This raises interesting questions for cases with large swell in the coastal zone.

On the basis of the measurements reported here, it could be argued that the wave-coherent heat flux simply contributes to the way the total flux is partitioned near the surface and is not an additional contribution to the total heat flux measured at some height above the surface. However, the simple model for scalar fluxes

supports the conclusion that this is an additional contribution to the air–sea heat flux. Furthermore, to the extent that current air–sea scalar flux parameterizations include surface wave dependence, wave-induced contributions are implicit in the parameterizations (cf. Fairall et al. 2003). However, a more complete set of measurements over a wide range of sea states and air–sea temperature differences is required to firmly establish the wave-induced contribution to the scalar fluxes.

The wind dependence of the phase in Fig. 6 suggests that there might be a sign reversal in wave-supported heat flux for very low and very high wind speeds. In either case, in the context of modeling efforts, our ability to understand the partitioning of the fluxes is paramount. For example, models that assume the sensible heat flux to be entirely supported by small-scale diffusion processes at the surface, without wave effects, would presumably make an error of approximately 5%–10%. Similarly, inverting the net heat flux to extract bulk-skin temperature corrections would also yield an error on the calculated ΔT, albeit to a lesser extent. Nevertheless, recent parameterizations of bulk-skin temperature differences take small-scale waves into consideration (Castro et al. 2003). Despite our ability to measure total heat flux in an accurate manner away from the surface, not being able to understand the partitioning and the parameters that influence it limits our ability to extrapolate and model heat fluxes at higher wind speeds. This is of significant interest for hurricane and extreme wind speed conditions (Emanuel 1995).

Finally, it should be noted that the results presented here are for wind and wave conditions that are in the range of global averages. Our results indicate that the contribution of surface waves to the total heat flux is comparable in magnitude to other climatically significant effects such as those resulting from increases in anthropogenic aerosols and greenhouse gases (Houghton et al. 2001; see also http://www.grida.no/climate/ipcctar/wg1/006.htm). This is interesting and certainly calls for more attention to be paid to wave effects, especially in light of Fig. 7, which shows a dependence on wind speed and wave height. This, among other things, indicates that in the context of global climate, feedback effects might also play a significant role.

Acknowledgments. We thank Jim Lasswell and Atle Jensen for their support of the field measurements. This research was supported by an NSF Grant (OCE 01-18449) to WKM and FV and an ONR (Physical Oceanography) Grant to WKM. We thank James Mueller for his constructive comments on a draft of the paper.

REFERENCES

Belcher, S. E., and J. C. R. Hunt, 1998: Turbulent flow over hills and waves. *Annu. Rev. Fluid Mech.,* **30,** 507–538.

Castro, S. L., G. A. Wick, and W. J. Emery, 2003: Further refinements to models for the bulk-skin sea surface temperature difference. *J. Geophys. Res.,* **108,** 3377, doi:10.1029/2002JC001641.

Chang, J. H., and R. N. Wagner, 1975: Laboratory measurement of surface temperature fluctuations induced by small amplitude surface waves. *J. Geophys. Res.,* **80,** 2677–2689.

Donelan, M. A., B. K. Haus, N. Reul, W. J. Plant, M. Stiassnie, H. C. Graber, O. B. Brown, and E. S. Saltzman, 2004: On the limiting aerodynamic roughness of the ocean in very strong winds. *Geophys. Res. Lett.,* **31,** L18306, doi:10.1029/2004GL019460.

Edson, J. B., and C. W. Fairall, 1998: Similarity relationships in the marine atmospheric surface layer for terms in the TKE and scalar variance budgets. *J. Atmos. Sci.,* **55,** 2311–2328.

——, A. A. Hinton, K. E. Prada, J. E. Hare, and C. W. Fairall, 1998: Direct covariance flux estimates from mobile platforms at sea. *J. Atmos. Oceanic Technol.,* **15,** 547–562.

——, C. J. Zappa, J. A. Ware, W. R. McGillis, and J. E. Hare, 2004: Scalar flux profile relationships over the open ocean. *J. Geophys. Res.,* **109,** C08S09, doi:10.1029/2003JC001960.

Emanuel, K. A., 1995: Sensitivity of tropical cyclones to surface exchange coefficients and a revised steady-state model incorporating eye dynamics. *J. Atmos. Sci.,* **52,** 3969–3976.

Ewing, G., and E. D. McAlister, 1960: On the thermal boundary layer of the ocean. *Science,* **131,** 1374–1376.

Fairall, C. W., E. F. Bradley, D. P. Rogers, J. B. Edson, and G. S. Young, 1996: Bulk parameterization of air-sea fluxes for Tropical Ocean–Global Atmosphere Coupled-Ocean Atmosphere Response Experiment. *J. Geophys. Res.,* **101,** 3747–3764.

——, ——, J. E. Hare, A. A. Grachev, and J. B. Edson, 2003: Bulk parameterization of air–sea fluxes: Updates and verification for the COARE algorithm. *J. Climate,* **16,** 571–591.

Houghton, J. T., Y. Ding, D. J. Griggs, M. Noguer, P. J. van der Linden, X. Dai, K. Maskell, and C. A. Johnson, Eds., 2001: *Climate Change 2001: The Scientific Basis*. Cambridge University Press, 881 pp.

Hristov, T., C. A. Friehe, and S. Miller, 1998: Wave-coherent fields in the air flow over ocean waves: Identification of cooperative behavior buried in turbulence. *Phys. Rev. Lett.,* **81,** 5245–5248.

Janssen, P. A. E. M., 1989: Wave-induced stress and the drag of air flow over sea waves. *J. Phys. Oceanogr.,* **19,** 745–754.

——, 1999: On the effect of ocean waves on the kinetic energy balance and consequences for the inertial dissipation technique. *J. Phys. Oceanogr.,* **29,** 530–534.

Jessup, A. T., and V. Hesany, 1996: Modulation of ocean skin temperature by swell waves. *J. Geophys. Res.,* **101,** 6501–6511.

Katsaros, K. B., 1980: The aqueous thermal boundary layer. *Bound.-Layer Meteor.,* **18,** 107–127.

Komen, G. J., L. Cavaleri, M. Donelan, K. Hasselmann, S. Hasselmann, and P. A. E. M. Janssen, Eds., 1994: *Dynamics and Modelling of Ocean Waves.* Cambridge University Press, 554 pp.

Kudryavtsev, V. N., and V. K. Makin, 2001: The impact of air-flow separation on the drag of the sea surface. *Bound.-Layer Meteor.,* **98,** 155–171.

Makin, V. K., and C. Mastenbroek, 1996: Impact of waves on air-sea exchange of sensible heat and momentum. *Bound.-Layer Meteor.,* **79,** 279–300.

——, and V. N. Kudryavtsev, 2002: Impact of dominant waves on sea drag. *Bound.-Layer Meteor.,* **103,** 83–99.

——, ——, and C. Mastenbroek, 1995: Drag of the sea surface. *Bound.-Layer Meteor.,* **73,** 159–182.

McAlister, E. D., 1964: Infrared-optical techniques applied to oceanography. I. Measurement of total heat flow from the sea surface. *Appl. Opt.,* **3,** 609–612.

Melville, W. K., 1996: The role of surface-wave breaking in air-sea interaction. *Annu. Rev. Fluid Mech.,* **28,** 279–321.

Miller, A. W., Jr., and R. L. Street, 1978: On the existence of temperature waves at a wavy air-water interface. *J. Geophys. Res.,* **83,** 1353–1365.

O'Brien, E. E., 1967: On the flux of heat through laminar wavy liquid layers. *J. Fluid Mech.,* **28,** 295–303.

Saunders, P. M., 1967: The temperature of the ocean–air interface. *J. Atmos. Sci.,* **24,** 269–273.

Simpson, J. J., and C. A. Paulson, 1980: Small-scale sea surface temperature structure. *J. Phys. Oceanogr.,* **10,** 399–410.

Sullivan, P. P., and J. C. McWilliams, 2002: Turbulent flow over water waves in the presence of stratification. *Phys. Fluids,* **14,** 1182–1195.

——, ——, and W. K. Melville, 2004: The oceanic boundary layer driven by wave breaking with stochastic variability. Part 1. Direct numerical simulations. *J. Fluid Mech.,* **507,** 143–174.

——, ——, and ——, 2007: Surface gravity wave effects in the oceanic boundary layer: Large-eddy simulation with vortex force and stochastic breakers. *J. Fluid Mech.,* **593,** 405–452.

Veron, F., W. K. Melville, and L. Lenain, 2008: Infrared techniques for measuring ocean surface processes. *J. Atmos. Oceanic Technol.,* **25,** 307–326.

Webb, E. K., G. I. Pearman, and R. Leuning, 1980: Correction of flux measurements for density effects due to heat and water vapor transfer. *Quart. J. Roy. Meteor. Soc.,* **106,** 85–100.

Witting, J., 1971: Effects of plane progressive irrotational waves on thermal boundary layers. *J. Fluid Mech.,* **50,** 321–334.

——, 1972: Temperature fluctuations at an air-water interface caused by surface waves. *J. Geophys. Res.,* **77,** 3265–3269.